Topics in Catalysis (2025) 68:1668–1681
https://doi.org/10.1007/s11244-025-02077-0

ORIGINAL PAPER

Sunlight-Driven (Eu, Pd, Fe, Bi) Modified-TiO_2 Photocatalysts and Their Catalytic Activity Using Scavengers Molecules

Dora Alicia Solis-Casados[1] · Susana Hernandez Lopez[1] · Tatiana E. Klimova[2] · Fernando Gonzalez-Zavala[1] · Luis Escobar-Alarcón[3]

Accepted: 7 February 2025 / Published online: 17 February 2025

Abstract

In this work, it is reported the physicochemical characterization and photocatalytic activity evaluation of TiO_2 thin films modified with Eu, Pd, Fe and Bi. Several characterization techniques were used to investigate thin film properties. The chemical composition as well as the chemical environment of the elements present were determined by X-ray photoelectron spectroscopy (XPS). The crystalline structure was characterized by X-ray diffraction (XRD) and micro-Raman spectroscopy (RS) whereas the optical band gap was determined using UV-Vis spectroscopy. The photocatalytic activity was evaluated in the degradation of the Malachite Green (MG) dye using simulated sunlight. It was found that films modified with Fe and Pd reached MG degradations close to 64.7 and 58.1% after 180 min of reaction. Additionally, thin films were photocatalytically evaluated under UV light (λ=254 nm) using wastewater containing diclofenac (DCF). The best catalytic performance (44% was reached by the film modified with Fe followed by the films modified with Pd (39%) and Bi (38%). To identify the role of reactive species for degradation of MG and DCF, triethanolamine (TEOA), isopropyl alcohol (IPA), ascorbic acid (AA) and benzoquinone (BZQ) were employed as scavenger's molecules. The results obtained revealed that the $O_2^{\bullet}$ radical is the reactive specie that mainly contributes to the MG and DCF degradation.

Graphical abstract

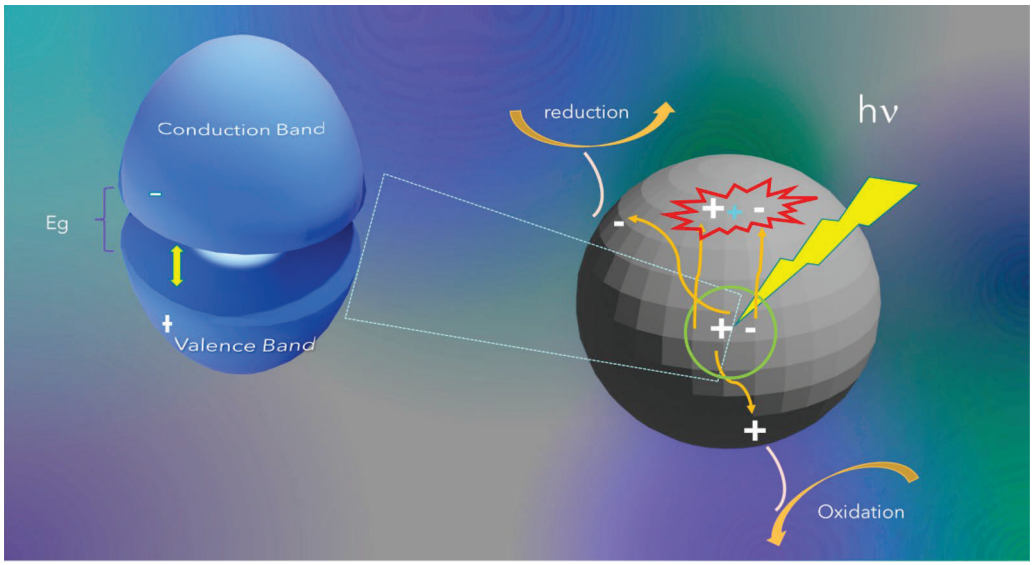

Keywords Films · Sol-gel · Photocatalysis · Scavengers · MG · Diclofenac

Extended author information available on the last page of the article

1 Introduction

Wastewater treatment has acquired great interest for researchers worldwide due to the necessity to obtain clean water for human consumption and for the different anthropogenic activities [1]. The photocatalytic process has proved to be a good option to address this issue through the degradation of organic pollutants, such as dyes and pharmaceutical drugs, contained in wastewaters. However, the efficiency of this process depends on the photocatalyst, among other parameters, which ideally should be active under sunlight irradiation and able to degrade the organic molecules towards their complete mineralization transforming them to CO_2 and H_2O. Several photocatalysts have been investigated seeking to increase their photocatalytic activity under solar light. Additionally, research has been carried out to understand how the photocatalysts work to degrade organic pollutants and to study the role of the reactive species using scavenger molecules [2–6]. The TiO_2 in its anatase crystalline phase is widely used as photocatalyst, due to its low cost, non-toxicity, stability and without any risk to the environment and living beings; nevertheless, its wide band gap energy close to 3.2 eV remains as its main drawback [7]. In most cases, the photocatalysts have been studied in powder form; however, in some applications, the use of powders could present additional problems among which can be mentioned the recovering of the powder from the photocatalytic reaction system; another problem is the agglomeration of the suspended particles which increases at high concentrations of photocatalyst, increasing the dispersion of the light used to activate the photocatalyst and consequently the overall efficiency of the photocatalyst is diminished. An alternative to avoid such problems is the use of immobilized photocatalysts in thin film form. On the other side, efforts to obtain titania based photocatalytic formulations, sensitive under visible light and preserving their photocatalytic activity have been investigated; among the proposed solutions, the narrowing of the band gap energy of the TiO_2 by its doping with transition metals, the coupling of semiconductors and the metal incorporation in the titania lattice have been reported [8–10]. Additionally, it is important to identify the role of the reactive species generated, specifically hydroxyl radicals ($OH^{\bullet}$), superoxide ($O_2^{\bullet}$) and holes (h^+) to degrade pollutant molecules and try to determine the photocatalytic degradation mechanism. In this work, it is reported the effect of incorporation of the Eu, Pd, Fe, and Bi in TiO_2, with the purpose of studying its photocatalytic response. Particularly, bismuth was chosen because it is a low-cost element abundant in Mexico and it is found in several compounds, for example as sodium bismuth, bismuthine and bismuth subsalicylates amongst others. Concerning the photocatalytic response, the effect of the metal incorporated in the titania on the role of the reactive species responsible for the degradation of the Malachite Green dye and diclofenac drug was investigated, for this purpose, scavenger molecules were added separately to the reaction system.

2 Experimental

2.1 Synthesis of TiO_2 Thin Films with Incorporation of Eu, Pd, Fe, and Bi

To obtain the TiO_2 thin films, the solutions were prepared by the sol-gel technique. This was done by mixing 1 mL of titanium isopropoxide with 10 mL of 2-propanol stirred for approximately 1 h. Thin films of TiO_2 modified with Pd, Fe, Bi and Eu were obtained by adding into the solution prepared previously one of the following salts: palladium(II) nitrate hydrate ($Pd(NO_3)_2 \cdot H_2O$, from Aldrich), iron(III) chloride hexahydrate ($FeCl_3 \cdot 6H_2O$, from Fermont), bismuth(III) nitrate pentahydrate ($Bi(NO_3)_3 \cdot 5H_2O$, J.T. Baker) and europium(III) nitrate ($Eu(NO_3)_3 \cdot 5H_2O$, Aldrich), respectively. The amounts of the first two salts were determined to produce nominal concentrations of PdO of 5, 10 and 20 wt% (corresponding to 0.49, 0.99 and 2.04 at% of Pd) and Fe_2O_3 of 5, 10 and 20 wt% (corresponding to 0.74, 1.48 and 3.0 at% of Fe) in the TiO_2. The amount of bismuth nitrate was calculated to give 5 and 20 wt% of Bi_2O_3 in the TiO_2 (corresponding to 0.2 and 0.82 at% of Bi). The amount of europium nitrate was calculated to give 10 and 20 wt% of Eu_2O_3 in the TiO_2 (corresponding to 0.55 and 1.12 at% of Eu). Thin films were obtained spreading each of the sol-gel solutions onto soda lime glass substrates ($25 \times 25 \times 1$ mm) by the spin coating technique. After deposition, the films were thermally treated at 450 °C for 4 h, except the film containing europium that was treated at 650 °C, this temperature was chosen to obtain Eu_2O_3 according to the thermogravimetric analysis graph for the $Eu(NO_3)_3 \cdot 5H_2O$ (not shown); additionally, this film was deposited on quartz substrate because 650 °C is above the glass transition temperature. These films (series 1) were used as photocatalysts to degrade the MG dye. A second group of films (series 2) was prepared using the same procedure described before but with the amount of the corresponding salt calculated to produce, in all cases, 20 wt% of the corresponding oxide in the TiO_2. This second group of films used as photocatalysts to degrade the diclofenac drug under UV-light irradiation was chosen because of the difficulty to degrade this organic molecule.

2.2 Thin Films Characterization

Thin films were characterized by several techniques to know their physical and chemical properties. X-ray photoelectron spectroscopy (XPS) was used to determine the elemental chemical composition of the films surface; wide and narrow spectra of each thin film were acquired with a JEOL JPS-9200 spectrometer equipped with an Al (K_α = 1486.6 eV) X-ray source. Narrow spectra were obtained to perform elemental quantification by the Specsurf software using the sensitivity factors method. The chemical shifts in the photoelectron spectrum were used to determine the chemical state of the elements present, and the full width at half maximum (FWHM) was used to separate overlapping peaks in cases where the signals were broad. The adventitious carbon (C1s) peak centered at 284.8 eV was used to adjust the photoelectron energy due to charge correction for each region of the elements present in the XPS spectra. UV-Vis spectroscopy was used to determine the band gap energy of the thin films applying the Tauc method to the transmittance spectra acquired using a Perkin Elmer Lambda 35 spectrophotometer. X-ray diffraction (XRD) was employed to identify the thin films crystalline phases, diffraction patterns were acquired using a Bruker D8 Advance Diffractometer. The microstructure of the thin films was characterized by micro-Raman spectroscopy, spectra were recorded using an HR LabRam 800 spectrometer equipped with a confocal microscope Olympus BX40 using a Nd: YAG laser beam (532 nm).

2.3 Photocatalytic Degradation Activity

The photocatalytic performance of the obtained thin films was evaluated following the degradation reaction of the malachite green (MG) dye as a model molecule of pollutant in wastewaters. This molecule was chosen because water pollution by dyes is an important problem around the world; specifically, the MG dye is one of the most used dyes in aquaculture, dentifrices, silk and paper tinction [11–13]. The photocatalytic reaction system was prepared by introducing a piece of 1 cm^2 of the photocatalyst thin film into 25 mL of an aqueous solution of 10 µmol/L of the MG dye. Afterwards, the reaction system was stirred for 15 min in dark conditions to establish the adsorption equilibrium between photocatalyst and the MG solution. Each photocatalyst was activated by illuminating it with the light emitted by a solar simulator (Sciencetech SF150 model, class A) at an average irradiance close to 60 mW/cm^2. The degradation degree of the MG dye was followed by the decrease of its characteristic absorption band peaking at 619 nm in the absorbance spectra by plotting the MG concentration as a function of the reaction time. Previously, a calibration curve of absorbance of the MG dye solution as a function of its concentration was determined. Then the natural logarithm of MG concentration versus reaction time was plotted to determine the kinetic rate constants using a pseudo-first order kinetic model. Total Organic Carbon (TOC) measurements were performed to assess the extent of mineralization. Diclofenac (DCF) pharmaceutical contained in a real wastewater was photodegraded in the same reaction system using an UV lamp (λ = 254 nm) as irradiation source to activate the photocatalyst, this wavelength was chosen due to the low reaction rate to degrade this molecule. The degradation degree of the DCF was followed by the decrease of its absorption band, with maximum at 198 nm, as a function of time. The kinetic rate constant considering a pseudo-first order model was obtained from natural logarithm of absorbance versus reaction time considering a pseudo-first order reaction.

In order to determine the preferential reaction route in the degradation of the investigated organic molecules, several scavenger-type molecules were employed: for the MG dye, benzoquinone (BZQ) was used to block the superoxide $O^{2\bullet}$ radicals, triethanolamine (TEOA) interacts with the holes (h^+) blocking them, and isopropanol (IPA) reacts with the hydroxyl radicals ($OH^\bullet$) impeding further reactions; in the case of DCF the scavengers used were: ascorbic acid (AA) to trap the superoxide radical, TEOA to block the holes and tertbutyl alcohol (TBA) to trap the hydroxyl radicals [3–6].

3 Results and Discussion

3.1 Thin Films Characterization

3.1.1 XPS Characterization

The chemical composition of the thin films in at% and wt%, for series 1 and series 2 is presented in Tables 1 and 2 respectively. In general terms, the atomic content of Ti and O agrees well with the stoichiometric values of TiO_2. For series 1, the atomic content of each element incorporated into the TiO_2 varies depending on the load of the corresponding salt used in the synthesis as was described in the experimental section, whereas for series 2, only one value of atomic content is reported in each case. Thin films were identified as M(x or y)–TiO_2, where M = Pd, Fe, Eu or Bi whereas x and y indicate the respective atomic percent corresponding to series 1 and 2 respectively.

A detailed analysis of the XPS spectra was performed to determine the chemical environment of the elements present in each film. Spectra were fitted using Voigt profile line shapes to resolve overlapping peaks and assigning them to the corresponding oxidation state.

Table 1 Chemical composition obtained by XPS of films of Series 1

(at%)											
Pd(x)–TiO_2			Bi(x)–TiO_2			Fe(x)–TiO_2			Eu(x)–TiO_2		
Ti	O	Pd	Ti	O	Bi	Ti	O	Fe	Ti	O	Eu
33.3	66.7	0	32.9	67.1	0	35.0	65.0	0	30	70	0
32.9	65.8	1.3	25.8	72.4	1.8	32.1	63.0	4.9	30	68.8	1.2
29.3	67.8	2.9	26.3	66.6	7.1	28.3	63.9	7.8	29	69.3	1.7
24.7	60.8	14.5				24.7	62.0	13.3			
(wt%)											
Pd(x)–TiO_2			Bi(x)–TiO_2			Fe(x)–TiO_2			Eu(x)–TiO_2		
Ti	O	Pd	Ti	O	Bi	Ti	O	Fe	Ti	O	Eu
59.90	40.10	0	59.46	40.54	0	61.70	38.30	0	56.18	43.82	0
56.94	38.06	5.00	44.59	41.83	13.58	54.52	35.77	9.71	52.81	40.48	6.71
50.16	38.80	11.04	33.06	27.98	38.96	48.16	36.35	15.49	50.38	40.24	9.38
31.97	26.30	41.73				40.53	34.01	25.46			

Table 2 Chemical composition obtained by XPS of films of Series 2

(at%)											
Pd(y)–TiO_2			Bi(y)–TiO_2			Fe(y)–TiO_2			Eu(y)–TiO_2		
Ti	O	Pd	Ti	O	Bi	Ti	O	Fe	Ti	O	Eu
26.2	67.0	6.8	27.0	69.5	3.5	27.5	71.0	1.5	29.1	69.3	1.6
(wt%)											
Pd(y)–TiO_2			Bi(y)–TiO_2			Fe(y)–TiO_2			Eu(y)–TiO_2		
Ti	O	Pd	Ti	O	Bi	Ti	O	Fe	Ti	O	Eu
41.12	35.15	23.73	41.21	35.46	23.33	51.9	44.79	3.3	50.75	40.39	8.86

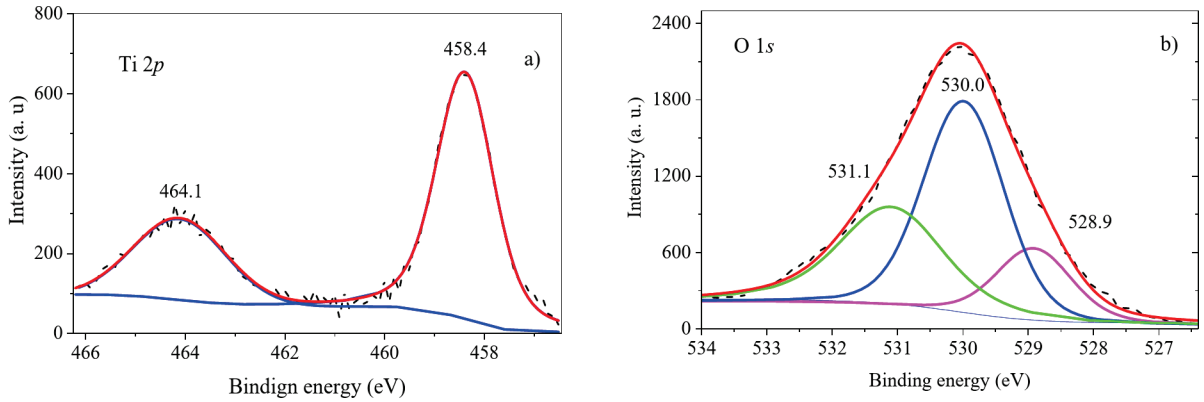

Fig. 1 Deconvolution of the XPS spectra of the M(x)–TiO_2 film, x = 0.0, of Series 1. **a** Ti 2p region, **b** O 1s region

Figure 1a shows the Ti 2p region of the pure TiO_2 film; the deconvolution of the experimental spectrum reveals a doublet with maxima at 458.4 and 464.1 eV attributed to the $2p_{3/2}$ and $2p_{1/2}$ orbitals. The values of FWHM, double-peak distance, and intensity ratio of spin-orbit splitting were in this case: 1.35, 5.7 and 2.08 respectively, which are characteristics of Ti–O bonds in TiO_2. [14, 15] The fitting parameters for the subsequent deconvolutions of the Ti 2p region were very close to the values used in this case.

The O 1s region shown in Fig. 1b was deconvoluted using Voigt peaks with the FWHM varying from 1.4 to 1.9 eV. These peaks located at 528.9, 530.0 and 531.1 eV are assigned in order of intensity as follows: the main peak at 530.0 eV is assigned to O–Ti (Ti^{4+}) in TiO_2 [16, 17], the peak at 528.9 eV corresponds to O^{2-} ions in oxygen deficient TiO_2 [18], and the peak at 531.1 eV can be assigned to OH groups [19] that probably were adsorbed due to air exposure of the samples.

When 7.1 at% of Bi is incorporated to the TiO_2 films, two doublets fits the Ti 2p region as is shown in Fig. 2a. The most intense at 458.4 and 464.2 eV is assigned to Ti-O bonds of TiO_2, the second one at 457.5 and 463.2 is assigned to Ti^{3+} in oxygen deficient TiO_2 (TiO_{2-x}). Figure 2b shows the Bi 4f region in which two doublets are observed, the first one at 157.9 and 163.2 eV is attributed to Bi^0 [20] whereas the second one at 162.0 and 156.7 eV could be assigned

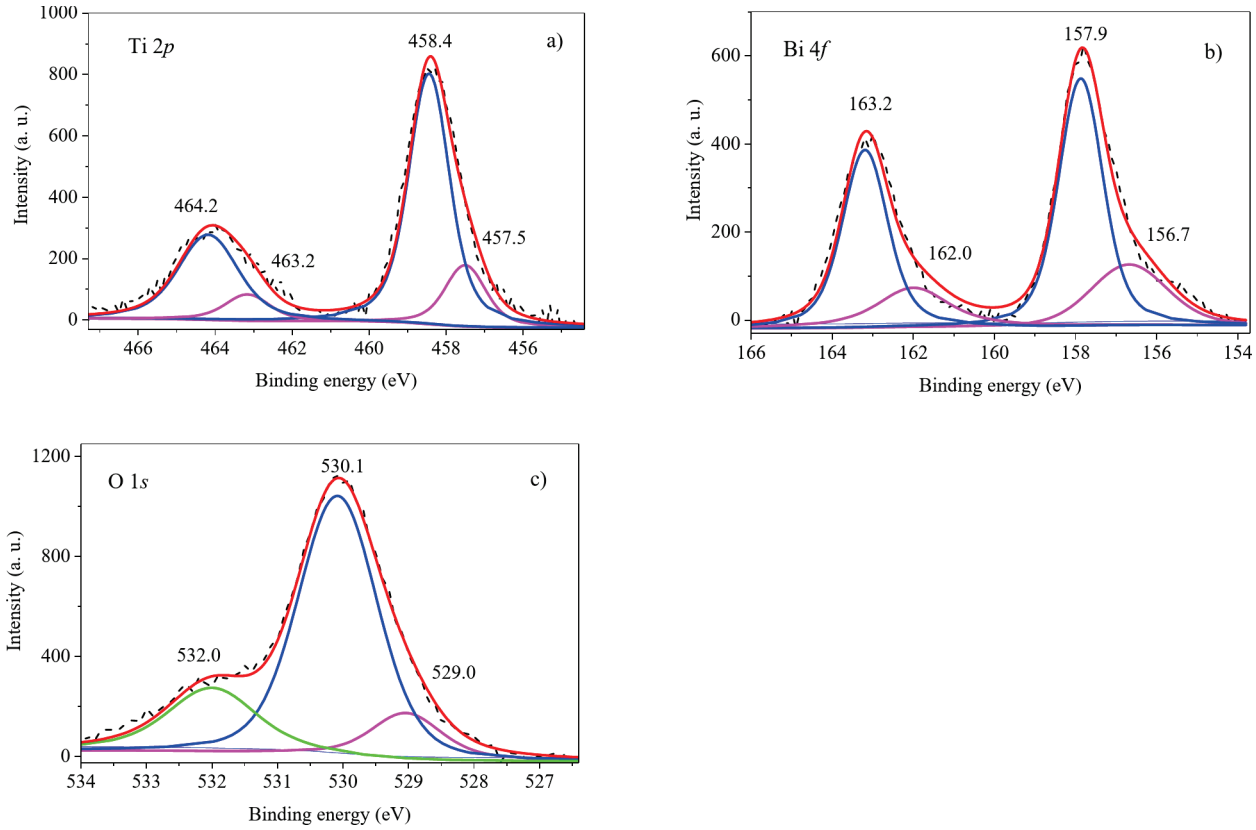

Fig. 2 Deconvolution of the XPS spectra of the Bi(7.1)–TiO_2 film, **a** Ti 2p region, **b** Bi 4f region, **c** O 1s region

to Bi: TiO_2 metal clusters (Bi^0) [21]. The O 1s XPS region shown in Fig. 2c reveals three peaks located at 529.0, 530.1 and 532.0 eV. The first peak located at 529.0 eV is assigned to the O^{2-} ions in oxygen deficient TiO_2 [18], the second peak at 530.1 eV is attributed to the O-Ti bond in the TiO_2; the third peak at 532.0 eV is due to adsorbed moisture from the environment [19].

Figure 3 shows the deconvolution of the XPS spectra of TiO_2 film modified with 14.5 at% of Pd revealing that incorporation of Pd to the titania produces some changes to the chemical environment of the present elements. Figure 3a shows the presence of two doublets in the Ti 2p region. Again, the most intense, with peaks at 458.4 and 464.1 eV, is attributed to the Ti-O bonds in the TiO_2 in its anatase phase; the second one at 457.8 and 463.5 eV is assigned to O^{2-} ions in oxygen deficient TiO_2 [18].

In Fig. 3b the Pd region shows the Pd $3d_{3/2}$ and $3d_{5/2}$ orbitals; two doublets are fitted in this case, the first one at 336.1 and 341.4 eV can be attributed to the Pd nanoparticles whereas the second one at 334.9 and 340.1 eV can be assigned to Pd^0 [22, 23]. Figure 3c shows the O 1s XPS region, three peaks were found for this spectrum at 529.1, 530.1 and 531.2 eV; as in the previous case, the first peak located at 529.1 eV is assigned to the O^{2-} ions in oxygen deficient TiO_2 [18], the second peak at 530.1 eV is attributed to the O-Ti bond in the TiO_2 and the third peak at 531.2 eV is due to adsorbed moisture from the environment.

When 1.7 at% of europium is incorporated to the TiO_2 thin film, the Ti 2p region (Fig. 4a) shows the same features observed in the previous samples, the main doublet attributed to Ti-O bonds of TiO_2 and the second one due to Ti^{3+} [24]. Figure 4b shows the deconvolution of the XPS spectrum of the Eu 3d region. An intense doublet at 1136.3 and 1165.7 eV reveals the presence of Eu^{3+} suggesting that Eu is dispersed as Eu_2O_3 outside of the TiO_2 structure [25]. Two doublets of lower intensity at 1125.5 and 1153.7 eV; and at 1128.9 and 1158.0 eV could be associated to Eu^{2+}.

The XPS spectrum in Fig. 4c for the O 1s region displays three peaks at binding energies of 529.2, 530.1 and 531.2 eV. The peak at 529.2 eV is attributed to O^{2-} ions as before [18]; the second peak at 530.1 eV is associated to Ti–O in TiO_2 [19], and the peak at 531.2 eV is assigned to adsorbed moisture from the environment.

Figure 5 presents the XPS spectra of the Fe (13.3)–TiO_2 thin film. The Ti 2p region showed in Fig. 5a display two doublets: the main due to the Ti–O bond in the Ti^{4+} oxidation state in TiO_2, the second one due to O^{2-} ions [18]. In Fig. 5b the XPS Fe region shows the $2p_{3/2}$ and $2p_{1/2}$ orbitals, two doublets are observed in this case, the first doublet at 711.7 and 724.9 eV attributed to Fe^{3+} in Fe_2O_3; the

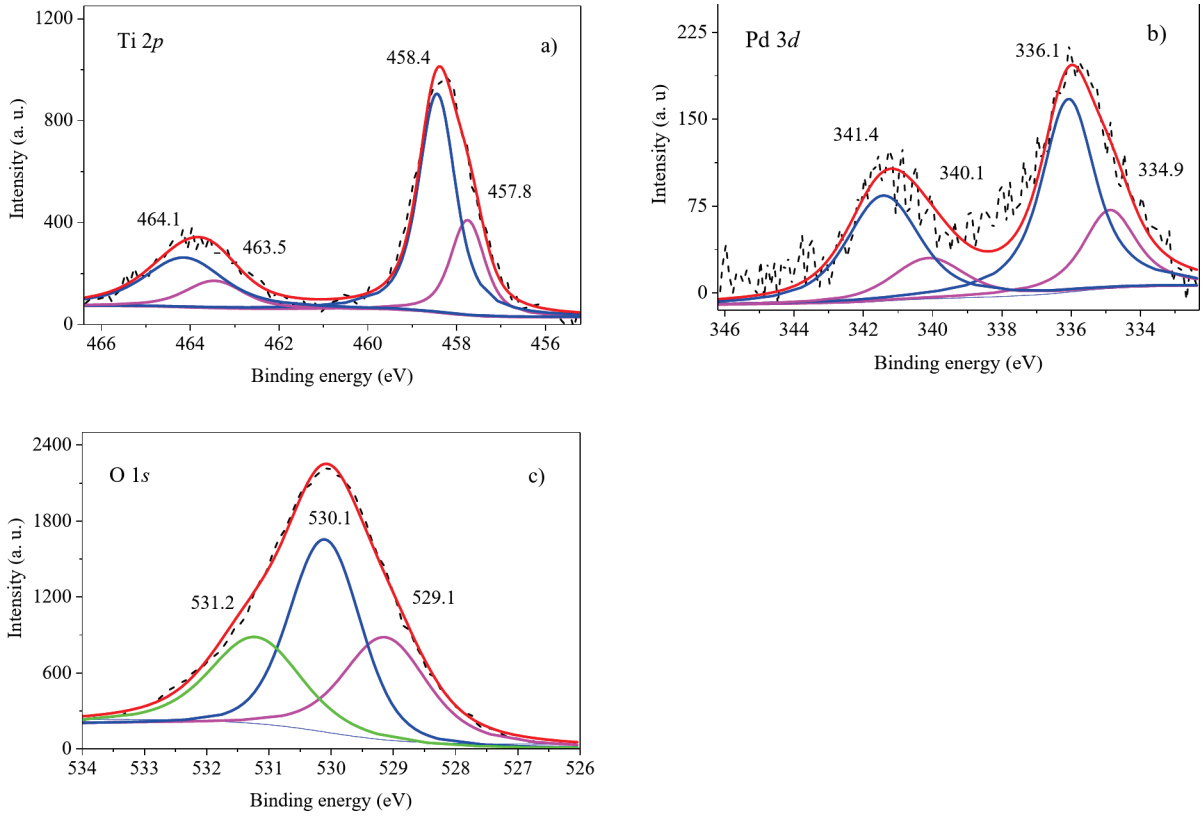

Fig. 3 Deconvolution of the XPS spectra of the Pd(14.5)–TiO_2 film, **a** Ti 2p region, **b** Pd 3d region, **c** O 1s region

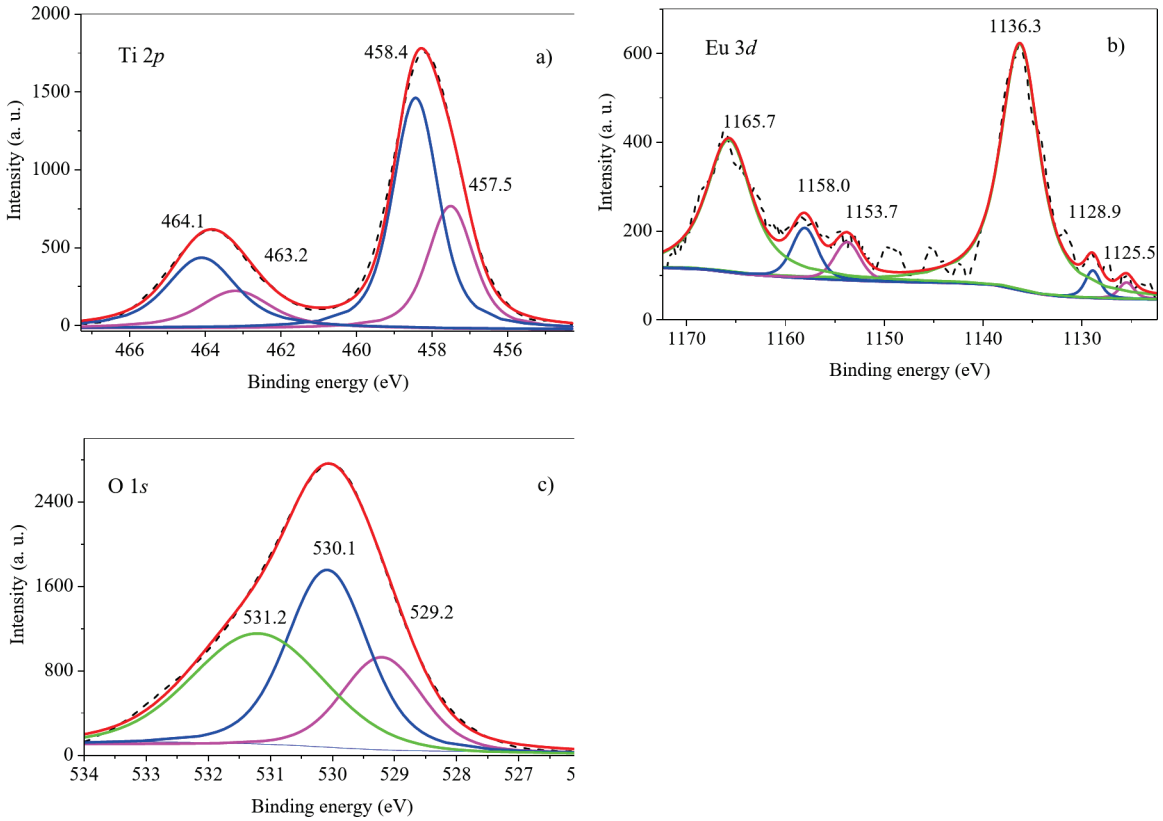

Fig. 4 Deconvolution of the XPS spectra of the Eu(1.7)–TiO_2 film, **a** Ti 2p region, **b** Eu 3d region, **c** O 1s region

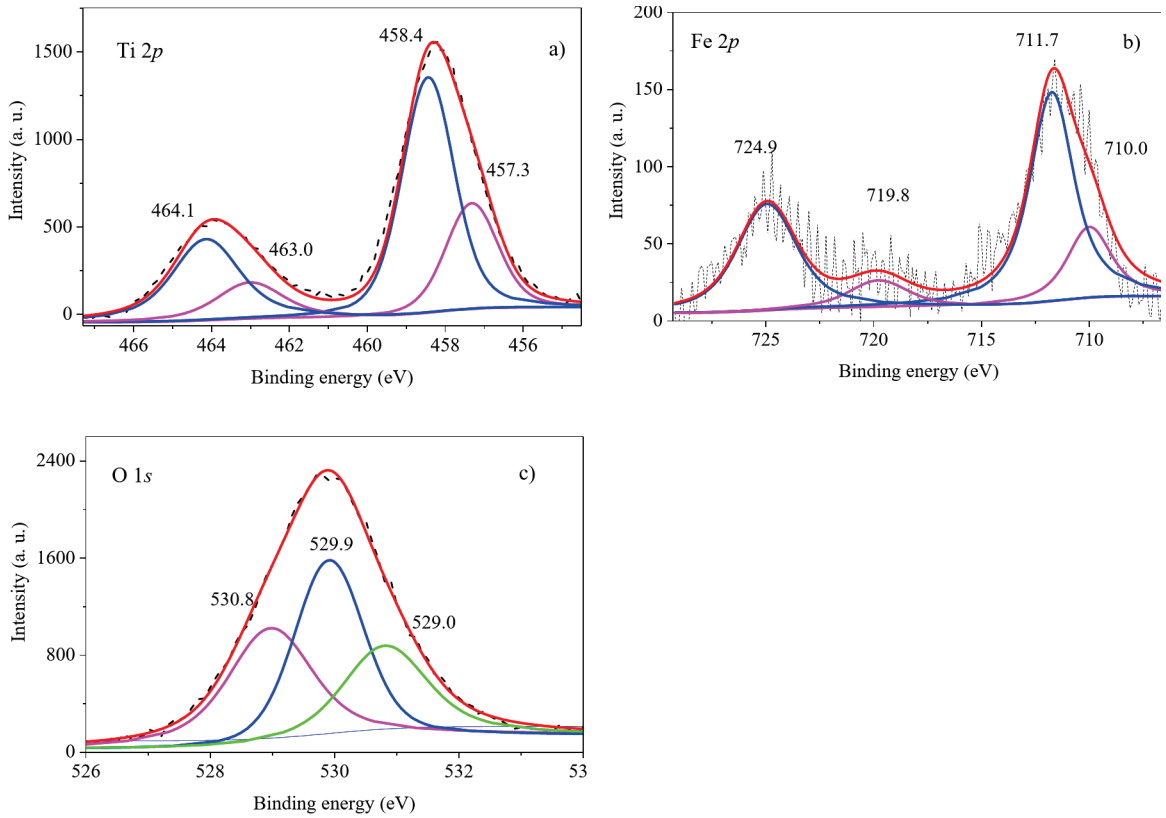

Fig. 5 Deconvolution of the XPS spectra of the Fe(13.3)–TiO_2 film, **a** Ti 2p region, **b** Fe 2p region, **c** O 1s region

second one at 710.0 and 719.8 eV could be assigned also to Fe–O bonds [26]. Figure 5c shows the O 1s region, three peaks located at 529.0, 529.9, 530.8 eV are observed. The first and second peaks at 529.0 and 529.8 eV are assigned to the O^{2-} ions and TiO_2 respectively, whereas the third can be assigned to OH groups that probably were adsorbed due to air exposure.

3.1.2 XRD Characterization

Characterization of the crystalline phases present in the thin films is shown in Fig. 6. Figure 6a shows the XRD patterns of the Pd(x)–TiO_2 films displaying diffraction lines at 2θ = 25.3°, 48.0° and 55.0°, characteristics of the anatase crystalline phase of titania (JCPDS 21-1272) corresponding to the (1 0 1), (2 0 0) and (2 1 1) planes respectively. No diffraction lines attributed to palladium, or any compound of this element are observed. This result indicates that incorporation of Pd to the TiO_2 lattice does not cause changes to its crystalline structure; however, an important effect is observed, as the Pd content increases the intensity of the diffraction lines decreases suggesting a loss of crystallinity. Figure 6b shows the XRD patterns of the Bi(x)–TiO_2 thin films. The TiO_2 thin film present diffraction lines at 2θ = 25.3° and 37.8°, corresponding to the anatase crystalline phase of titania (JCPDS 21-1272). The diffraction patterns of the Bi modified thin films show that Bismuth induces the transformation of the anatase phase to new crystalline phases of bismuth titanates, at 7.1 at% of Bi, diffraction lines at 2θ = 27.7°, 30.4°, 31.8°, 34.8°, 38.01° reveal the apparition of $Bi_{12}TiO_{20}$ (JCPDS 78-1158). The XRD characterization of the Fe(x)–TiO_2 and Eu(x)–TiO_2 thin films is not reported because their diffraction patterns did not show any peak. Concerning the films of the series 2 their XRD patterns are presented in Fig. 6c, all of them show diffraction lines at 2θ= 25.3°, 37.9°, 48.1°, 53.8°, 55.1°, 62.7°, 68.9°, 70.2°, 75.1°, characteristics of the anatase phase of titania (JCPDS 21-1272); the thin film containing Pd, shows three low intensity additional diffraction lines at 34.5°, 55.6° and 72.7° due to palladium oxide accordingly to the JCPDS 02-1432 card.

3.1.3 Raman Spectroscopy Characterization

Figure 7 shows the Raman spectra of samples corresponding to series 1. All spectra display Raman features at 142, 196, 396, 516 and 638 cm^{-1} revealing that TiO_2 in the anatase phase [27] is present in all samples. In general terms, no matter the metal used to modify the TiO_2 the main vibrational feature of anatase at 142 cm^{-1} presents shifts suggesting the introduction of the metal in the anatase lattice. The Raman

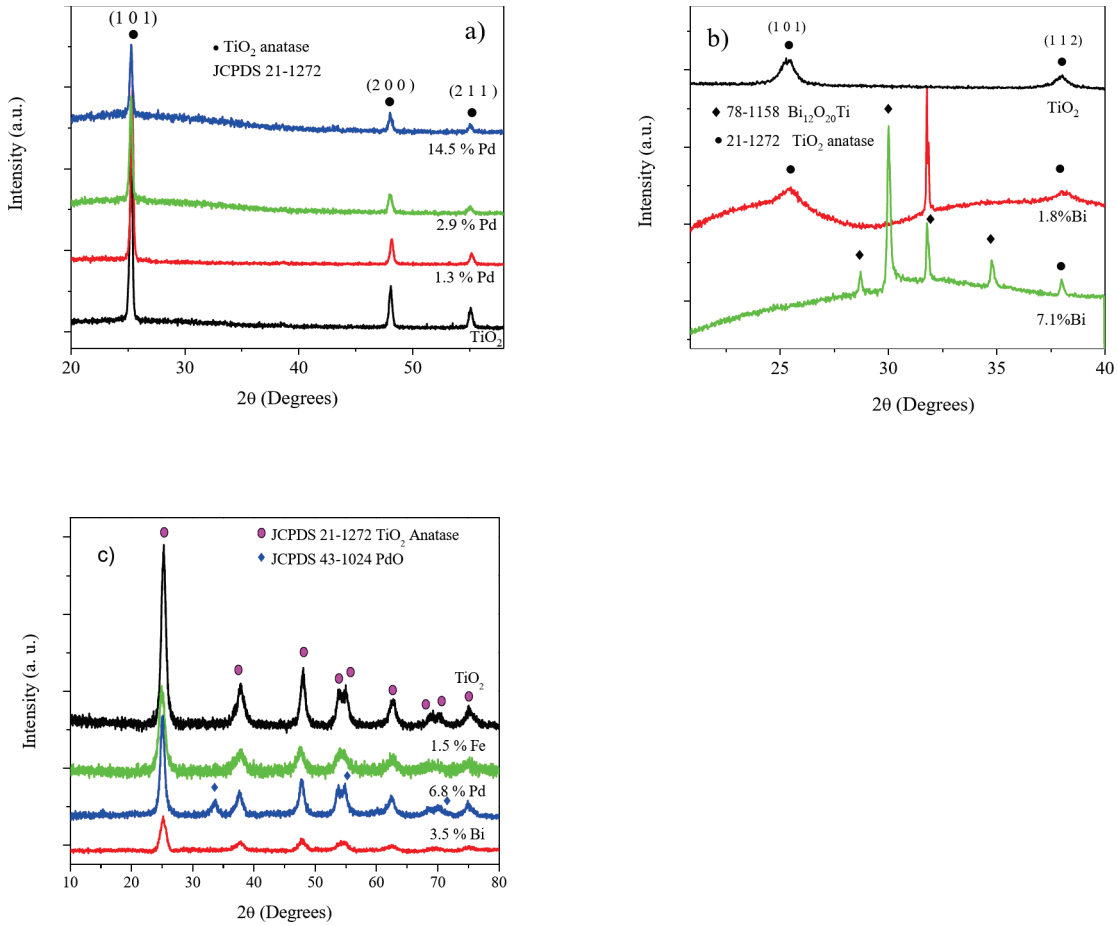

Fig. 6 XRD patterns corresponding to: **a** Pd(x)–TiO_2, **b** Bi(x)–TiO_2 thin films of series 1, and **c** XRD of M(y)–TiO_2 films of series 2

spectra of the Eu(x)–TiO_2 samples (Fig. 7c) show that due to the higher thermal treatment temperature used for this film (650 °C) a mixture of the anatase and rutile phases is present. Raman spectra of samples of series 2 (Fig. 8), show in all cases, vibrational Raman features at 144, at 197, 396, 516, 638 cm^{-1} revealing as expected that the anatase phase is present. Also, as in series 1, in all Raman spectra the peak at 144 cm^{-1} shifts its maximum suggesting the introduction of the metal in the anatase lattice (Fig. 8b).

3.1.4 UV-Vis Characterization

The band gap energy values, determined from the UV-Vis spectra using the Tauc Model [28], are shown in Table 3 for samples of series (1) It is seen that when Palladium is incorporated in the TiO_2 the band gap energy decreases to values as low as 2.3 eV indicating that this sample can absorb wavelengths lower than 539 nm taking advantage of a major proportion of the solar spectrum. The band gap energy of the photocatalysts Fe(x)–TiO_2 and Eu(x)–TiO_2 remains close to 3.5 eV, found for the TiO_2 thin film, suggesting that iron and europium incorporation does not change the electronic structure of TiO_2, however, it could affect other properties such as charge carrier dynamics, surface reactivity or light absorption. Table 4 shows the band gap energy (Eg) values determined from the UV-Vis spectra for samples of series (2) In this case, band gap decrease from 3.6 eV (TiO_2) to 3.4 eV (Pd (6.8)–TiO_2 film). In case of films containing Bi or Fe, two absorption edges were found, in these cases, two energy band gap values were estimated and are reported in Table 4; the Fe (1.5)–TiO_2 film has band gap energies of 3.5 and 2.9 eV whereas the Bi (3.5)–TiO_2 film has band gap energies of 3.5 and 1.7 eV, similar to the reported in [29].

3.2 Photocatalytic Activity of the Malachite Green (MG) dye

Figure 9 shows the MG degradation degrees reached using the prepared photocatalysts until a reaction time of 180 min. For comparison purposes the photocatalysts with the highest photocatalytic activity were chosen. It is also shown the degradation degree reached by the photolysis process as reference. It is observed that the Fe (4.9)–TiO_2 and the Pd (14.5)–TiO_2 photocatalysts reach the higher degradation

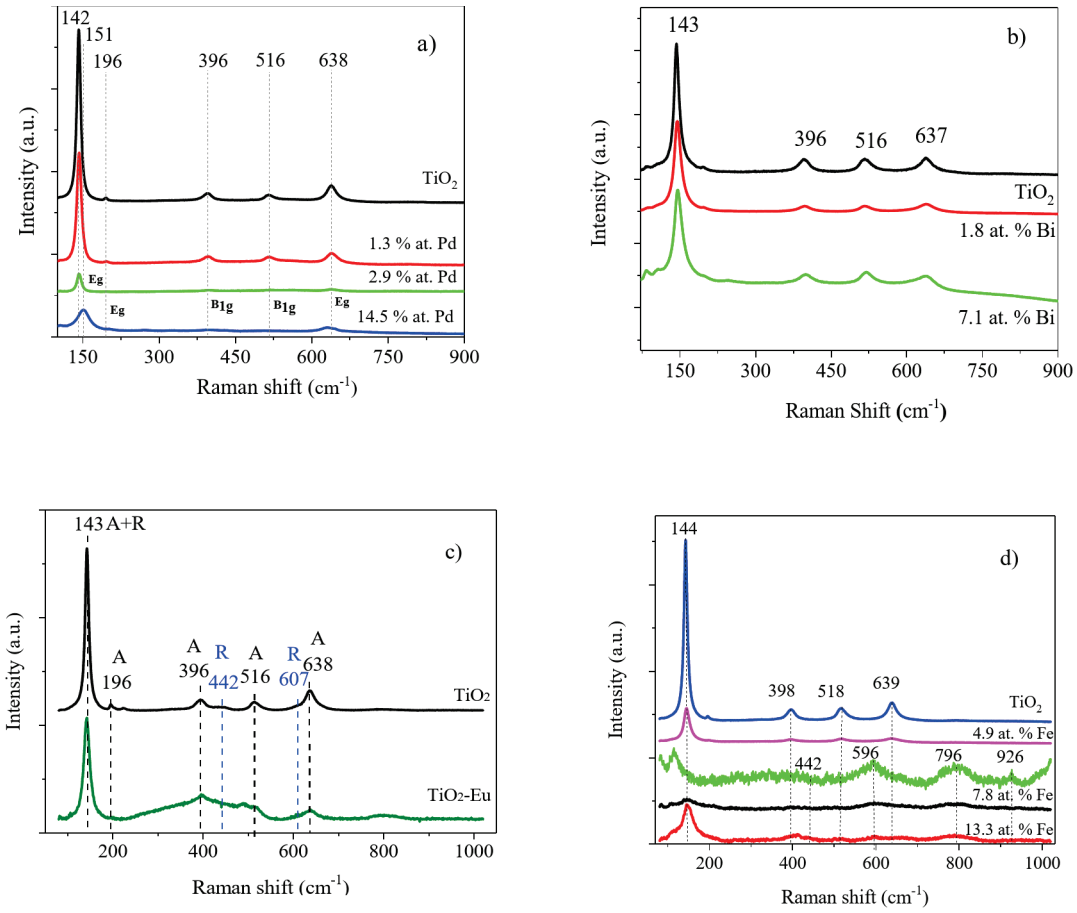

Fig. 7 Raman spectra of thin films of series 1, **a** Pd(x)–TiO_2, **b** Bi(x)–TiO_2, **c** Eu(x)–TiO_2, and **d** Fe(x)–TiO_2

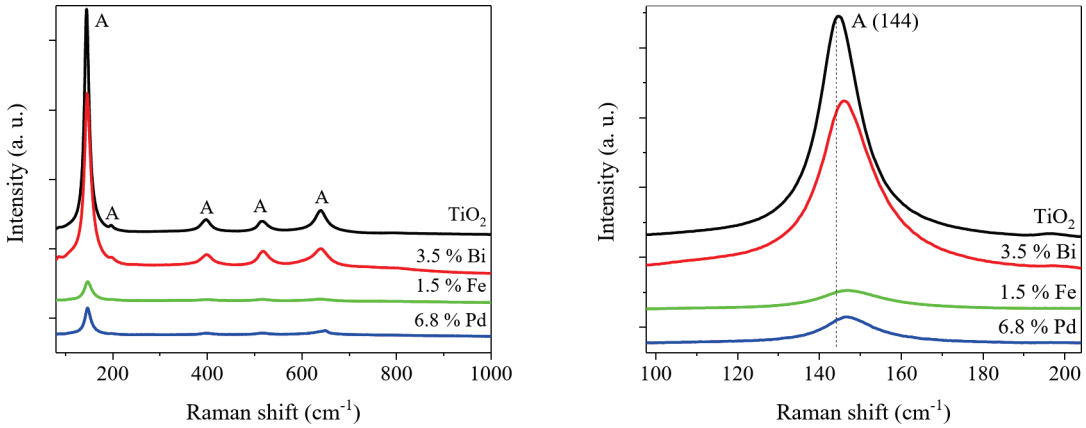

Fig. 8 Raman spectra of thin films series 2 **a** M(y)–TiO_2, **b** peak at 144 cm^{-1}

Table 3 Optical band gap energy (E_g) of the thin films of Series 1

Pd (at%)	E_g (eV)	Bi (at%)	E_g (eV)	Fe (at%)	E_g (eV)	Eu (at%)	E_g (eV)
0	3.3	0	3.3	0	3.6	0.0	3.5
1.3	3.2	1.8	3.4	4.9	3.6	1.7	3.5
2.9	3.1	7.1	3.2	7.8	3.6	1.9	3.5
14.5	2.3	–	–	13.3	3.5	–	–

Table 4 Optical band gap energy (E_g) of the thin films of Series 2

Thin film	E_g (eV)
TiO_2	3.6
Bi (3.5 at%)–TiO_2	3.5, 1.8
Fe (1.5 at%)–TiO_2	3.5, 2.9
Pd (6.8 at%)–TiO_2	3.4

degree, 64.7% and 58.1% respectively, after 180 min of reaction time. The Eu(x)–TiO_2 photocatalyst shows a conversion degree very similar to the uncatalyzed process. In order to determine that mineralization is occurring, TOC measurements were performed at the end of the photocatalytic reaction. Figure 10 shows the comparison of the TOC results with the degradation degrees obtained from absorbance measurements as well as the difference between these two data. In general terms, it is seen that both values are very close, suggesting that the prepared photocatalysts mineralize the MG dye almost completely. In all cases the degradation degrees obtained from the absorbance measurements are higher than the TOC determinations suggesting that a little fraction of the MG molecule does not reach the complete mineralization. The differences between these data span from 3 to 12% revealing that the Pd modified TiO_2 film has a better performance for mineralization, followed by Bi–TiO_2 > Eu–TiO_2 > TiO_2 > Fe–TiO_2. These results indicate that modification of TiO_2 with Fe, Bi and Pd improves the photocatalytic response of TiO_2 in 53%, 76% and 61% respectively and more important improves the mineralization of the MG dye.

The degradation reactions were carried out at the same conditions using scavenger molecules TEOA, IPA and BZQ to gain insight about the preferential reaction pathways followed in each case. These scavengers help in identifying the reactive species involved in the photocatalytic process. The participation of $O_2^{\bullet}$ was determined using the benzoquinone (BZQ) molecule. The role of $OH^{\bullet}$ radicals was determined with isopropanol as scavenger. Finally, the contribution to the degradation due to h^+ was revealed by adding triethanolamine (TEOA) to the reaction system. Figure 11 shows the kinetic rate constants, for the different scavengers, determined considering a kinetic model of pseudo-first order. It is clearly observed that the degradation reaction increases when TEOA is added blocking the holes (h^+), which favors the availability of electrons (e^-) and reduces O_2 to form superoxide radicals, therefore the increase in the photocatalytic activity can be attributed to the superoxide radicals. When benzoquinone (BZQ) is added to the reaction system the MG degradation is completely inhibited confirming that the superoxide radicals are responsible of the degradation of the MG molecule. When IPA is added the kinetic rate constants decreases compared to the system without scavengers, suggesting a minor contribution of $OH^{\bullet}$ radicals to the degradation reaction [2–6].

3.3 Photodegradation of the Diclofenac (DCF) drug

The Diclofenac degradation degree, using as photocatalysts the films of series 2, is shown in Fig. 12. The maximum

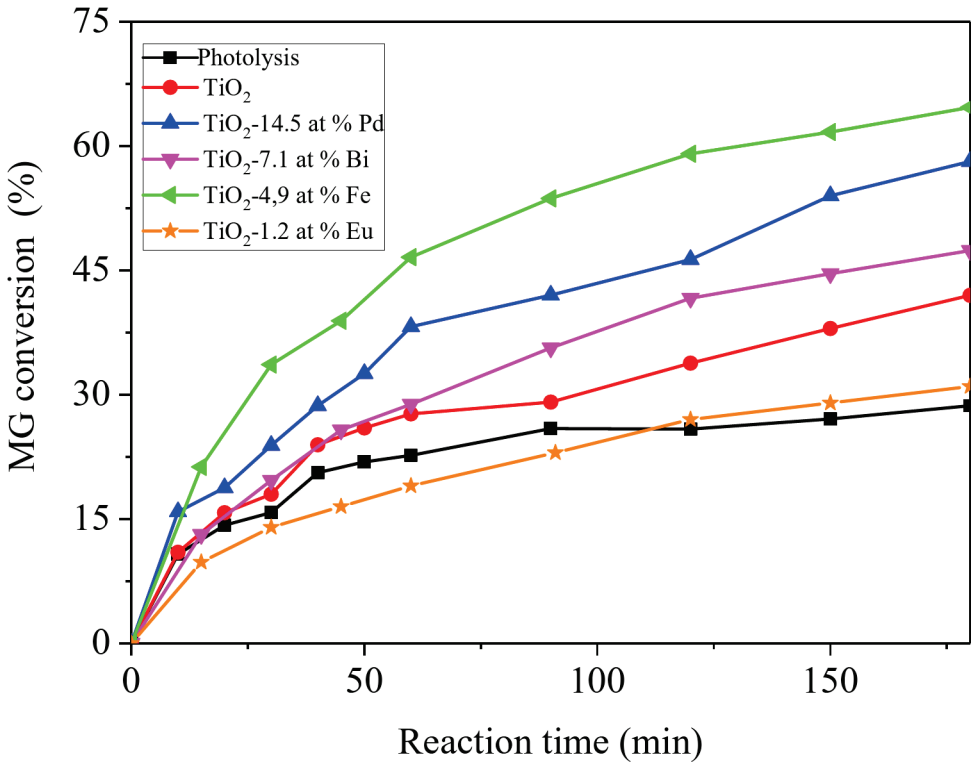

Fig. 9 MG degradation degree using the TiO_2, Pd–TiO_2, Bi–TiO_2, Eu–TiO_2, Fe–TiO_2 photocatalysts (series 1), the photolysis process is included as reference

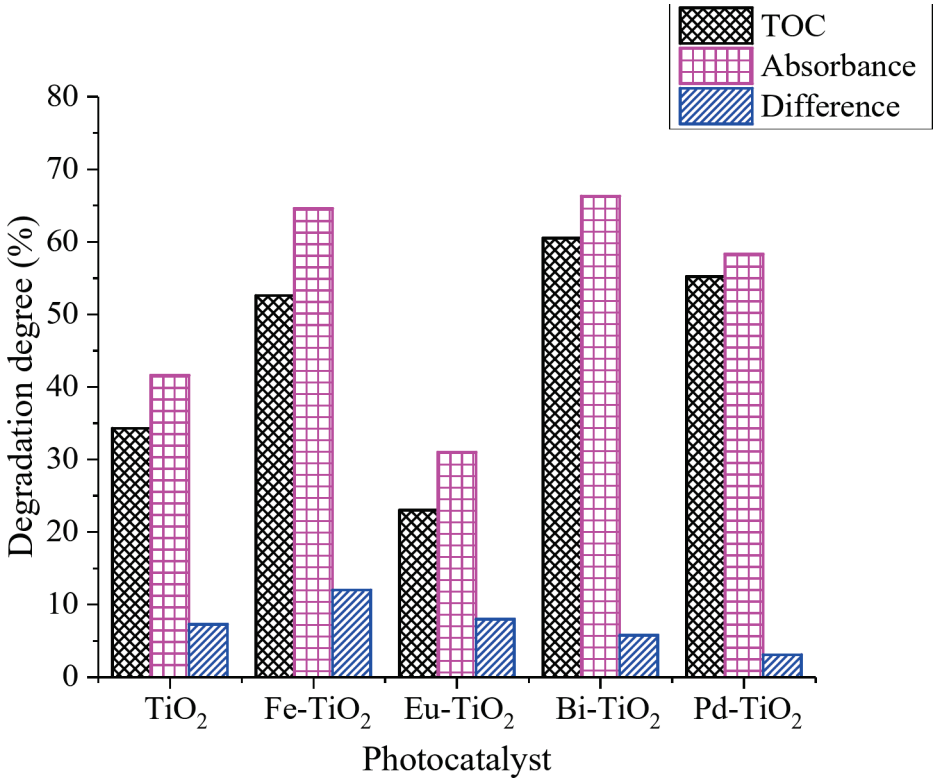

Fig. 10 Mineralization degree of MG dye by Total Organic Carbon (TOC) and absorbance measurements using the different photocatalysts of the series 1

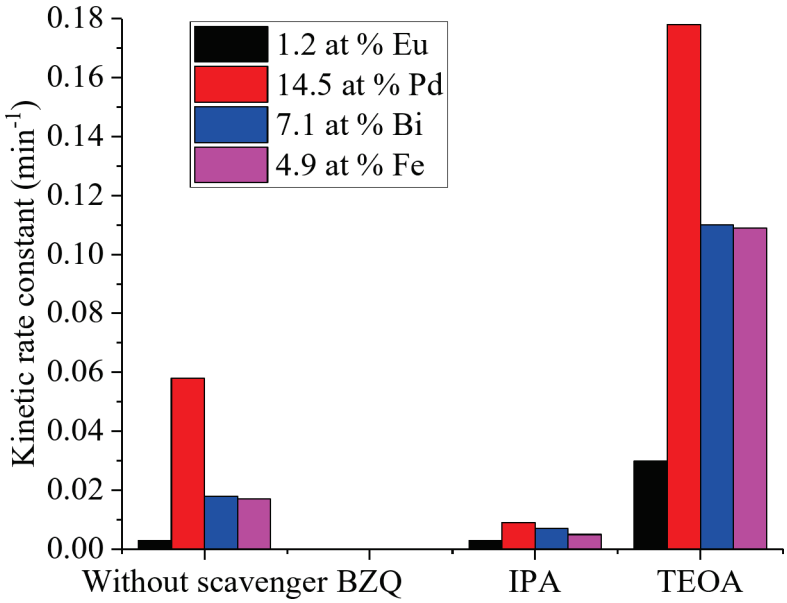

Fig. 11 MG degradation kinetic rate constants using scavenger molecules and the Pd–TiO_2, Bi–TiO_2, Eu–TiO_2, Fe–TiO_2 photocatalysts (series 1)

reaction time was 180 min and the photodegradation degree reached by the photolysis process is included as reference.

It is observed that the Fe (1.5)–TiO_2 photocatalyst reaches the highest degradation degree (43.1%) whereas Pd (6.8)–TiO_2 and Bi (3.5)–TiO_2 films reach 39% and 38% of degradation respectively. The TiO_2 photocatalyst has the lower photocatalytic activity reaching 36% of DCF degradation.

These results indicate addition of Fe, Bi and Pd to TiO_2 improves 22% the photocatalytic response of TiO_2 and increases 50% respect the uncatalyzed process. To gain insight about the role that play each reactive specie, the degradation reactions were carried out at the same conditions using as scavenger molecules TEOA, TBA and AA. The participation of superoxide radicals $O_2^{\bullet}$ was determined using the ascorbic acid (AA) molecule, which is another scavenger molecule with similar reactivity such as the benzoquinone (BZQ). The role of $OH^{\bullet}$ radicals was determined with tertbutyl alcohol (TBA) as scavenger with the same

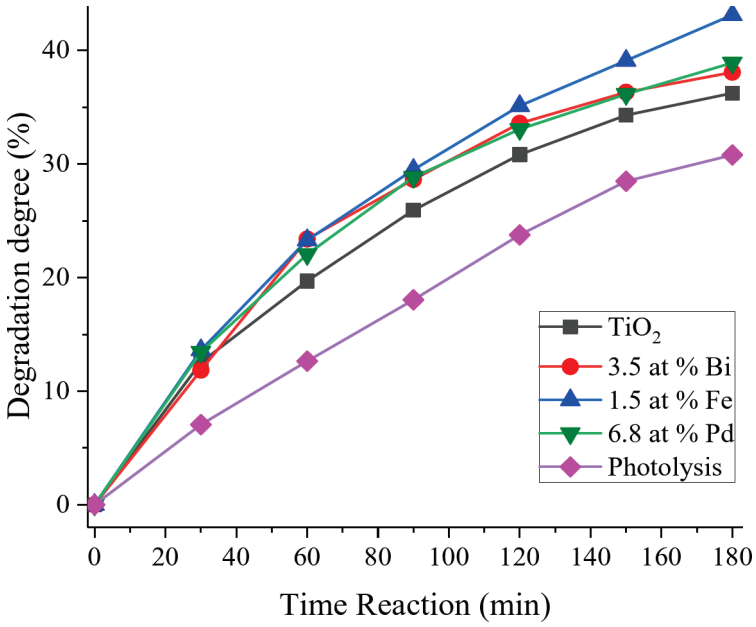

Fig. 12 DCF degradation degree using the TiO_2, Pd–TiO_2, Bi–TiO_2, and Fe–TiO_2 photocatalysts of series 2

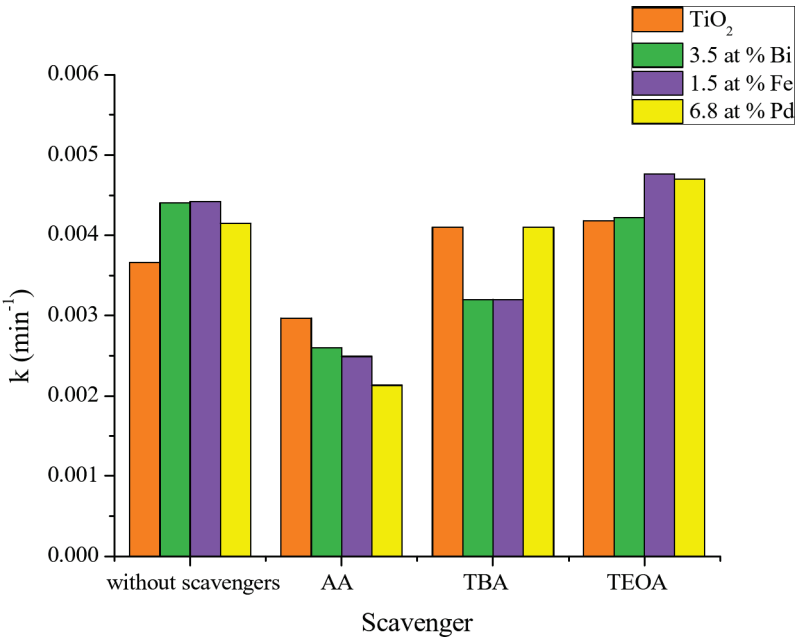

Fig. 13 DCF kinetic rate constants using scavenger molecules for the different photocatalysts of series 2

reactivity such as isopropyl alcohol (IPA). Finally, the contribution to the degradation due to h^+ was revealed by adding triethanolamine (TEOA) to the reaction system. Figure 13 shows the kinetic rate constants, for the different scavengers, determined considering a kinetic model of pseudo-first order. When Ascorbic acid (AA) is incorporated into the reaction system the DCF degradation decreases. Incorporation of TEOA to the reaction system block the holes h^+, that favors electrons availability for the degradation, observed in Fig. 13, with the constant increase in kinetic rate. This result besides the previous one reveals that diclofenac degradation is driven by the superoxide radicals $O_2^{\bullet}$. The incorporation of TBA to the reaction system results in a low kinetic rate constant for the Fe–TiO_2 and Bi–TiO_2 photocatalysts referred to the process without scavenger, there is seen that $OH^{\bullet}$ radicals contribute in a low proportion to the degradation reaction.

The photocatalytic results can be correlated with the physicochemical characterization as follows: in general terms structural and optical properties remain without important changes due to the metal incorporation in the titania; however, the chemical state of Ti and O changes due to the incorporation of Bi, Pd, Eu and Fe according to the XPS results; Specifically, for the Ti 2p region, it is observed in all cases the presence of a signal close to 457.5 eV assigned to Ti^{3+} in oxygen deficient TiO_2 (TiO_{2-x}) that increase the

optical absorption [30]; the intensity of the signal corresponding to Ti^{3+} increases in the different samples as follows: TiO_2 < Bi(7.1)–TiO_2 < Pd(14.5)–TiO_2 < Fe(4.9)–TiO_2, in good agreement with the photocatalytic results. In the case of the O 1s region, the signal close to 529 eV corresponding to O^{2-} ions in oxygen-deficient regions in the TiO_2 lattice promoted by the presence of Ti^{3+} can be related to oxygen vacancies that favor the transfer of photogenerated electrons diminishing the electron-hole recombination [31]; in this case the intensity of the signal corresponding to O^{2-} ions increases following the same tendency, in good agreement with the observed for the Ti^{3+}. These results can explain the increase of the photocatalytic response observed. The Eu(1.7)–TiO_2 sample lies out of this behavior probably due to the presence of Eu_2O_3 outside of the TiO_2 structure.

4 Conclusions

(Eu, Pd, Fe, Bi) modified-TiO_2 photocatalysts in thin film form were obtained depositing sol solutions by the spin coating technique on glass substrates. These thin films showed photocatalytic activity for the degradation of malachite green dye under simulated sunlight. Particularly, the Fe and Pd modified-TiO_2 photocatalysts showed the best photocatalytic performance reaching MG degradation degrees close to 64.7 and 58.1% respectively, after 180 min of reaction time. The use of scavenger molecules to gain insight about the preferential reaction pathway indicates that the MG degradation is through superoxide radicals.

Acknowledgements D. Solis acknowledge to the SIEA-UAEM for financial support through the project UAEM-6853/2023 and COMECyT FICDTEM-2023-108. Also D. Solis thanks the technical assistance of LIA Citlalit Martínez Soto, Dr. Diego Martínez-Otero, Dr. Uvaldo Hernández-Balderas, M. en C Nieves Zavala, M. en C. Lizbeth Triana, M. en C. Melina Tapia, M. en C. Alejandra Núñez; F. González-Zavala thanks DGAPA-UNAM for his postdoctoral grant, and thanks to CONAHCyT for the posdoctoral fellowship at "Estancias Posdoctorales por México 2022".

References

1. Chong MN, Jin BC, Christopher WK, Saint C (2010) Water Res 44(10):2997–3027
2. Sherryna A, Tahir M, Zakaria ZY (2024) Int J Hydrogen Energy 51:1511–15312
3. Naranthatta MC, Pullanhi A, Malikayil ST (2025) React Kinet Mech Cat 138:375–391
4. Meiyazhagan S, Kavitha ER, Yugeswaran S, Santhanamoorthi N, Jiang G, Suresh K (2023) J Water Process Eng 55:104190
5. Kim H, Jang D, Choi S, Kim J, Park S (2021) Chemosphere 273:129731
6. González-Zavala F, Escobar-Alarcón L, Solís-Casados DA, Espinosa-Pesqueira M, Haro-Poniatowski E, Rodríguez-Castellón E, Rodríguez-Aguado E (2018) Catal Today 305:102
7. Nur ASM, Sultana M, Mondal A, Islam S, Robel FN, Islam A, Sumi MSA (2022) J Water Process Eng 47:102728
8. Carp O, Huisman CL, Reller A (2004) Progr Solid State Chem 32:33–177
9. Sayılkan F, Asilturk M, Tatar P, Kiraz N, Arpac¸ E, Sayılkan H (2007) J Hazard Mater 148:735–744
10. Crişan M, Gartner M, Szatvanyi A, Zaharescu M (2002) Rev Roumaine Chim 47(1–2):123–130
11. Akpan UG, Hameed BH (2009) J Hazard Mater 170(2–3):520–529
12. Srivastava S, Sinha R, Roy D (2004) Aquat Toxicol 66(3):319–329
13. Pérez-Estrada LA, Agüera A, Hernando MD, Malato S, Fernández-Alba AR (2008) Chemosphere 70(11):2068–2075
14. Sánchez-Zambrano KS et al (2022) Materials 15(9):3117
15. Pärna R et al (2011) Appl Surf Sci 257:6897–6907
16. Yamashita T et al (2008) Appl Surf Sci 254:2441–2449
17. Aronniemi M et al (2007) Appl Surf Sci 253:9476–9482
18. Grahmann CR, Pilleux ME, Fuenzalida VM (1994) J Am Ceram Soc 77(6):1601–1604
19. Dharmadhikari VS, Sainkar SR, Badrinarayan S, Goswami A (1982) J Electron Spectrosc Relat Phenom 25:181–189
20. Jovalekic C, Zdujic M, Atanasoska LJ (2009) J Alloys Compd 469(1–2):441–444
21. Wang L, Ma W (2013) Proc Environ Sci 18:547–558
22. Goetz J, Volpe MA, Sica AM, Gigola CE, Touroude R (1995) J Catal 153:86–93
23. Brun M, Berthet A, Bertolini JC (1999) J Electron Spectrosc Relat Phenom 104:55–60
24. Wagner N, Brümmer O, Sauer N (1982) Cryst Res Technol 17(9):1151–1158
25. Cho EJ, Oh SJ (1999) Phys Rev B 59:24:613–616
26. Yamashita T, Hayes P (2008) Appl Surf Sci 254:2441–2449
27. Picquard M, Escobar-Alarcón L, Torres E, Lopez T, Haro-Poniatowski E (2002) J Mater Sci 37:3241–3249
28. Makuła P, Pacia M, Macyk W (2018) J Phys Chem Lett 9:6814–6817
29. Escobar-Alarcón L, Solís-Casados DA, González-Zavala F, Romero S, Fernandez M, Haro-Poniatowski E (2017) J Phys Conf Ser 792(18):012006
30. Yang Y, Yin L-C, Gong Y, Niu P, Wang J-Q, Gu L, Chen X, Liu G, Wang L, Cheng HM (2018) Adv Mater 30:1704479
31. Chen Y, Fu X, Peng ZA (2023) Metals 13:1163

Authors and Affiliations

Dora Alicia Solis-Casados[1] · Susana Hernandez Lopez[1] · Tatiana E. Klimova[2] · Fernando Gonzalez-Zavala[1] · Luis Escobar-Alarcón[3]

✉ Dora Alicia Solis-Casados
solis_casados@yahoo.com.mx

[1] Facultad de Química, Universidad Autónoma del Estado de México, Centro Conjunto de Investigación en Química Sustentable UAEM-UNAM, Toluca, Mexico

[2] Facultad de Química, Departamento de Ingeniería Química, UNAM, Ciudad de Mexico, Mexico

[3] Departamento de Física, Instituto Nacional de Investigaciones Nucleares, Ocoyoacac, Mexico